A STATISTICAL STUDY OF HARD X-RAY FOOTPOINT MOTIONS IN LARGE SOLAR FLARES

A STATISTICAL STUDY OF HARD X-RAY FOOTPOINT MOTIONS IN LARGE SOLAR FLARES

YA-HUI YANG[1], C. Z. CHENG[1,2], SÄM KRUCKER[3], R. P. LIN[3,4], AND W. H. IP[5]
[1] Plasma and Space Science Center, National Cheng Kung University, Tainan 70101, Taiwan; yhyang@pssc.ncku.edu.tw, frankcheng@pssc.ncku.edu.tw
[2] Department of Physics, National Cheng Kung University, Tainan 70101, Taiwan
[3] Space Sciences Laboratory, University of California, Berkeley, CA 94720-7450, USA; krucker@ssl.berkeley.edu, rlin@ssl.berkeley.edu
[4] Department of Physics, University of California, Berkeley, CA 94720-7450, USA
[5] Institute of Astronomy, National Central University, Jhungli 32001, Taiwan; wingip@astro.ncu.edu.tw

ABSTRACT

A statistical analysis of the temporal evolution of hard X-ray (HXR) footpoint motions in 27 M- and X-class solar flares observed by the Reuven Ramaty High Energy Solar Spectroscopic Imager is presented. Extreme UV images from TRACE and SOHO/EIT, Hα images, and magnetograms from SOHO/MDI are used to put the HXR footpoint motions in context of flare ribbons and the magnetic neutral line. Footpoint motions are often found to be complex making a statistical analysis difficult. In an attempt to simplify the analysis, each event was searched for motions predominantly parallel and predominantly perpendicular to the neutral line or flare ribbons. Four kinds of complex motions are described and their relationships to the possible magnetic reconnection processes are discussed. In the soft X-ray (SXR) rise phase, motions along the neutral line or flare ribbons are most common (20 out of 27) and only two events show perpendicular motions (for the remaining five events a simple classification was not possible). However, at later times around the SXR peak, perpendicular motion is more frequently observed ($\sim 40\%$) than motions along the neutral line or ribbons $\sim 27\%$. The preference of HXR kernels appearing at the footpoints of highly-sheared magnetic loops at the start of the SXR rise phase is consistent with the magnetic reconnection theory that the reconnection occurring at sheared magnetic arcade field lines produces most HXR energy release in the impulsive phase of large flares.

Key words: Sun: flares – Sun: X-rays, gamma rays

1. INTRODUCTION

Hard X-ray (HXR) emission in the solar surface is produced by the flare-accelerated electrons that precipitate from the corona and then lose their energy via collisions with ambient plasma in the chromosphere. Such HXR emissions appear as kernels at the footpoints of magnetic loops and are most prominently observed in the impulsive phase. It is believed that magnetic reconnection in the corona is responsible for the energy release of solar flares, but the details of how electrons are accelerated are presently not understood. Since the reconnection process occurring in the corona is difficult to observe directly, the HXR sources can be regarded as the chromospheric signatures of progressive reconnection in the corona. HXR footpoints and their apparent motion thus provide information on the temporal evolution of the reconnection process.

According to the classical CSHKP magnetic reconnection model (Carmichael 1964; Sturrock 1966; Hirayama 1974; Kopp & Pneuman 1976); for a review see (Priest & Forbes 2002), increasing separation of flare ribbons is expected as the outer arcade magnetic field lines reconnecting successively at higher and higher altitudes. Such a feature with footpoints moving perpendicularly outward from a neutral line has also been found in many HXR observations (Sakao et al. 1998; Liu et al. 2004; Bogachev et al. 2005; Krucker et al. 2005; Veronig et al. 2006). Nevertheless, converging motion with decreasing separation in HXR sources was also observed in large flares (Sakao et al. 1998; Fletcher & Hudson 2002; Ji et al. 2006). Ji et al. (2006) explain such a feature as the signature of a fast relaxation of sheared magnetic field from the corresponding decrease of shear angle. In addition, HXR kernel motions along neutral lines were also noticed in previous studies (Fletcher & Hudson 2002; Krucker et al. 2003; Siarkowski & Falewicz 2004; Bogachev

et al. 2005; Grigis & Benz 2005). Under the assumption that the HXR kernels are located at the conjugate footpoints of newly reconnected field lines that have the strongest reconnection rate (or reconnection electric field), such motion patterns could be referred as the movement of magnetic reconnection sites in different shearing degrees of field lines or just the propagation of accelerated plasma along a series of arcade field lines (Grigis & Benz 2005).

Choe & Cheng (2000) investigated the evolution of flare-associated arcade magnetic fields in a bipolar active region based on resistive MHD simulations by imposing various motion patterns of arcade field line footpoints. They found that when arcade field lines are sheared along the neutral line direction, a current sheet would form above a critical shear value producing the magnetic reconnection. On the other hand, when a converging footpoint motion is imposed on the pre-sheared arcade field lines, the magnetic shear also increases resulting in the current sheet formation and causing subsequent magnetic reconnection. However, if the shearing footpoint motion is followed by a diverging motion, the magnetic reconnection process would slow down and eventually ceases.

Sakao et al. (1998) analyzed the separation between HXR footpoints in 14 flares using Yohkoh/HXT observations (Kosugi et al. 1991) and found that there is no preference for the diverging motion. A similar result was also obtained in the subsequent study by Bogachev et al. (2005). They analyzed qualitatively the position changes of conjugate HXR footpoints with respect to the corresponding neutral lines during flares. All Yohkoh flares in their study were cataloged according to three fundamental types: (1) footpoints moving away from each other in the nearly perpendicular direction to a neutral line (Type I), (2) footpoints moving mainly along a neutral line in the opposite direction (Type II), and (3) footpoints moving mainly along a

neutral line in the same direction (Type III). Type I motion is consistent with the prediction of the CSHKP model that the magnetic reconnection occurs progressively toward outer arcade field lines resulting in the diverging footpoint motions. The magnetic reconnection in Type II motion would take place in arcade field lines of different magnetic shear degrees and thus produces the shearing footpoint motions. Type III motion could result from the displacement of particle acceleration region via a disturbance propagating along a series of arcade field lines, which is probably related to an eruptive filament (Grigis & Benz 2005). Only 13% of selected 31 flares in Bogachev et al. (2005) show the distinct Type I motion, while about 61% flares show the motion pattern along a neutral line. They thus propose that the standard flaring model is too simple to explain the main features of flares. On the other hand, it should be mentioned that the separation distances between two conjugate HXR footpoints could vary with arcade morphology. Thus, tracing HXR footpoints throughout the flare comparing with the available ribbon morphology in EUV/UV or Hα would be more appropriate in describing and understanding the magnetic reconnection process.

More detailed investigations of flare-associated HXR footpoint motions have been achieved in specific flares with high cadence and high spatial-resolution measurements by the Reuven Ramaty High Energy Solar Spectroscopic Imager (RHESSI; (Lin et al. 2002). Systematic but more complex HXR footpoint motion patterns are found to be the common feature in large flares. However, a statistical and quantitative analysis of temporal and spatial evolution of RHESSI HXR footpoint motions in different phases of flares has not been carried out yet so far. Different from previous investigations, we particularly focus on the tendency of motion patterns in the SXR rise phase of flares, during which most nonthermal energy is released and particles are accelerated. In this study, 27 well observed M- and X-class flares by RHESSI during 2002–2005 in combination with TRACE, EIT, Hα, and MDI measurements are analyzed to identify the motion patterns of HXR footpoints in different flare phases. The selection criteria of flare events and analysis method are described in Section 2. The statistical results of motion patterns in different flaring phases are presented in Section 3. Discussion and summary are given in Section 4.

2. EVENT SELECTION AND ANALYSIS

The HXR sources in this study are obtained from RHESSI images reconstructed with the CLEAN algorithm (Hurford et al. 2002) using grids $3 \sim 6$ ($\sim 10''$ FWHM) and ~ 12 s integration time (i.e. three times of RHESSI rotation period). To avoid the pulse pileup of lower energy photons (e.g., Smith et al. 2002), only the emissions above 30 keV (i.e., energy range of 30–60 keV or 50–100 keV) are used. Periods within 20 s after an attenuator change are excluded to avoid the appearance of artifacts in CLEAN maps. The footpoint positions are obtained by fitting a two-dimensional elliptical Gaussian to each HXR source individually. The line-of-sight neutral line is identified from the nonsaturated MDI magnetogram near the time when HXR sources are first seen in CLEAN maps. The corresponding ribbon morphology is obtained from TRACE EUV images or high-resolution Hα images recorded by the global network. The EIT images are used instead if no appropriate TRACE or Hα data is available.

According to the GOES $1 \sim 8$ Å measurements, there are 634 flare events greater than M-class from 2002 February to 2005 December. To minimize the projection effect in the MDI magnetogram, only those flares occurring between E70° and W70° are selected as our candidates, which yields a list of 466 flares. Since we are mainly concerned with the evolution of HXR footpoints in the impulsive phase, flares with complete coverage of RHESSI HXR observations or with partial coverage of RHESSI HXR measurements in the rise phase of GOES soft X-ray (SXR) lightcurves are selected. There are 255 flares sorted out in this step. Moreover, at least five successive images with two separately distinct HXR footpoints in CLEAN maps are required in each event to trace their evolution of motion patterns. As a result, a total of 27 flares with available MDI magnetograms, EUV/UV, or Hα observations satisfy all the above selection criteria, as listed in Table 1.

For simplification, the HXR footpoint motions in this study are divided into two groups: (1) HXR footpoints mainly moving perpendicularly to the neutral line, including the diverging or converging motions, and (2) HXR footpoints moving preferentially along the neutral line, including the movements in the same direction or opposite directions. We particularly focus on the preference of motion patterns in different time intervals of HXR emission enhancements. To characterize the motion patterns in different flaring phases, the whole RHESSI observing period in each event is divided into several time intervals depending on the temporal variations of HXR and SXR emissions and the corresponding motion patterns. According to the lightcurves of GOES SXR emissions, each divided time interval is then grouped to the SXR rise or main/gradual phases and analyzed separately. Such a division could illustrate the tendency of motion pattern in each time interval more distinctly while avoiding the problem of insufficient data points in most cases. Moreover, such analysis can highlight the patterns of the magnetic reconnection in the impulsive phase of HXR flares. To recognize the motion patterns quantitatively, the regression line for each HXR footpoint in every time interval is obtained by fitting the footpoint positions in each divided period individually. This vector is then decomposed to the parallel and perpendicular components with respect to the regression line of the corresponding line-of-sight neutral line obtained from the MDI magnetogram. The ribbon morphology from EUV/UV or Hα observation is also used for identification. However, it should be mentioned that it is still difficult to catalog the HXR footpoint motions due to the asymmetric emissions in the HXR footpoints, the difficulty of identifying the conjugate footpoints in multiple HXR sources, the complex configuration of neutral line, and the observational limitation for flares far from the solar center. Therefore, our purpose is to perform an analysis of the successive movements of HXR footpoints and relate them to the enhancements of HXR emissions rather than to classify their motion patterns exactly.

Two methods are applied for image co-alignment between different instruments. The TRACE white light (WL) images are aligned with the MDI continuum images first by fitting the sunspot positions if the corresponding WL image is available. The TRACE EUV/UV images together with the MDI magnetograms, which have the same pointing information as TRACE WL and MDI continuum images, are then aligned to the RHESSI CLEAN maps by fitting the associated features such as the saturated parts in EUV/UV images and the HXR kernels. If the corresponding TRACE WL image is unavailable, the EUV/UV images and the MDI magnetograms are aligned to the RHESSI CLEAN maps individually and manually. Moreover, the projection effect is removed before analyz-

Table 1
Summary of the Flares Studied

ID	Date	GOES (hh:mm) Start Peak End	RHESSI (hh:mm:ss) Obs. Period	HXR (keV)	AR#	Class	M_R, M_{MG}[a]	M_{Fp1}[b] (E/N)	M_{Fp2}[b] (W/S)	Counts[c] $\|_R, \perp_R, \|_{MG}, \perp_{MG}$
01	20020314	01:38 01:50 02:02	01:41:30∼01:53:38	30–60	9866	M5.7	∥(2), ⊥(1)	∥,∥,x	∥,∥,⊥	4,0,0,1
02	20020317	10:11 10:19 10:24	10:13:25∼10:18:04	30–60	···	M1.3	∥(1), ∥(1)	∥,∥	∥,∥,⊥	2,0,2,0
03	20020410	18:48 19:07 19:15	19:02:51∼19:04:30	30–60	9899	M1.6	∥(1), −(0)	∥	∥	2,0,0,0
04	20020726	22:03 22:17 22:32	22:06:49∼22:09:15	30–60	···	M5.3	∥(2),−(0)	∥, ∥	x,x	2,0,0,0
05	20020729	10:27 10:44 11:13	10:38:14∼10:40:04	30–60	···	M4.7	∥(1), −(0)	∥	∥	2,0,0,0
06	20020822	01:47 01:57 02:05	01:50:50∼01:54:10	30–60	0069	M5.4	∥(2), −(0)	∥,x	x,∥	2,0,0,0
07	20020910	14:49 14:56 15:00	14:52:24∼14:53:39	30–60	0105	M2.9	∥(1), −(0)	∥	∥	2,0,0,0
08	20021109	13:08 13:23 13:36	13:12:00∼13:22:01	30–60	0180	M4.6	∥(3), −(0)	∥,∥	∥,x,x	4,0,0,0
09	20021110	03:04 03:21 03:35	03:10:00∼03:13:12	30–60	0180	M2.4	x(2), −(0)	∥,∥	⊥,⊥	2,2,0,0
10	20021204	22:41 22:49 22:57	03:10:00∼03:13:12	30–60	0180	M2.5	∥(1), −(0)	∥	∥	2,0,0,0
11	20030423	00:39 01:06 01:15	01:01:24∼01:06:52	30–60	0338	M5.1	∥(1), x(1)	∥,∥	∥,⊥	2,0,1,1
12	20030529	00:51 01:05 01:12	00:59:02∼01:08:11	30–60	0365	X1.2	∥(3), x(1)	∥,∥,⊥,⊥	x,x,∥,∥	3,1,1,1
13	20030617	22:27 22:55 23:12	22:45:03∼22:59:24	30–60	0386	M6.8	∥(3), x(1)	x,∥,∥,∥	x,x,x,⊥	2,0,1,1
14	20031029	20:37 20:49 21:01	20:40:24∼20:58:29	50–100	0486	X10	∥(2),⊥(1)	∥,⊥,⊥	∥,x,⊥	2,1,0,2
15	20031101	22:26 22:38 22:49	22:29:30∼22:33:45	30–60	0486	M3.2	∥(2), −(0)	∥,∥	∥,⊥	3,1,0,0
16	20031102	17:03 17:25 17:39	17:15:00∼17:25:20	50–100	0486	X8.3	∥(2), ∥(1)	∥,∥,∥	x,∥,∥	3,0,2,0
17	20040406	12:30 13:28 13:46	13:21:39∼13:25:45	30–60	0588	M2.4	x(1), ⊥(1)	∥,x	⊥,⊥	1,1,0,1
18	20040912	00:04 00:56 01:33	00:32:28∼00:38:02	30–60	0672	M4.8	x(2), −(0)	∥,∥	⊥,⊥	2,2,0,0
19	20041103	03:23 03:35 03:57	03:28:13∼03:35:06	30–60	0696	M1.6	x(2), x(1)	∥,⊥,∥	∥,⊥,⊥	2,2,1,1
20	20041104	22:53 23:09 23:26	22:53:12∼23:05:46	30–60	0696	M5.4	⊥(4), −(0)	⊥,⊥,x,⊥	∥,⊥,x,∥	2,4,0,0
21	20041110	01:59 02:13 02:20	02:08:03∼02:11:42	30–60	0696	X2.5	∥(1),−(0)	∥	∥	2,0,0,0
22	20050101	00:01 00:31 00:39	00:27:49∼00:36:11	50–100	0715	X1.7	x(2), ⊥	⊥,∥,x	⊥,∥,⊥	2,2,0,1
23	20050115	22:25 23:02 23:31	22:39:22∼23:07:36	50–100	0720	X2.6	∥(2),x(1)	∥,⊥,⊥	∥,∥,∥	3,1,1,1
24	20050117	06:59 09:52 10:07	09:43:12∼09:57:44	50–100	0720	X3.8	∥(2), ⊥(2)	⊥,∥,⊥,⊥	∥,∥,⊥,⊥	3,1,0,4
25	20050119	10:19 10:24 10:29	10:20:12∼10:24:39	30–60	0720	M2.7	∥(1), ⊥(1)	∥,⊥	x,⊥	1,0,0,2
26	20050120	06:36 07:01 07:26	06:40:24∼06:54:57	50–100	0720	X7.1	∥(2), ∥(1)	∥,∥,∥	x,⊥,x	2,1,1,0
27	20050803	04:54 05:06 05:11	04:58:24∼05:05:50	30–60	0794	M3.4	⊥, ∥(1)	⊥,∥	⊥,∥	0,2,2,0

Notes.

[a] M_R and M_{MG} represent the motion patterns in the SXR rise and main/gradual phases, where the ∥, ⊥, and x indicate the parallel/antiparallel motion, perpendicular motion, and the motion patterns hard to classify, respectively.

[b] M_{Fp1} and M_{Fp2} represent the motion patterns for footpoints 1 (eastern/northern) and 2 (western/southern) in divided time intervals.

[c] The numbers of divided time intervals showing the parallel/antiparallel motion in the SXR rise phase ($\|_R$), the perpendicular motion in the SXR rise phase ($\perp_R$), the parallel/antiparallel motion in the SXR main/gradual phase ($\|_{MG}$), and the perpendicular motion in the SXR main/gradual phase ($\perp_{MG}$).

ing by converting the positions from Sun-center to heliographic coordinates.

3. RESULTS

It must be emphasized that the movements of HXR footpoints can be much more complicated than the three types introduced in Section 1. Nonetheless, this study tries to provide a general picture of HXR footpoint motions by tracing their evolution throughout the entire flaring period in order to provide information for understanding magnetic reconnection processes.

Figure 1 illustrates one kind of complex HXR motions, in which two conjugate HXR footpoints move preferentially along the neutral line or ribbons first and then move away from each in the nearly perpendicular direction. The time profiles of 4 s averaged HXR flux obtained from RHESSI 30–60 or 50–100 keV and 3 s averaged GOES SXR flux in 1–8 Å are shown as the thick and thin curves respectively in the upper panel of Figures 1(a)–(d). The divided time intervals to differentiate the motion patterns in different flaring periods are represented by the horizontal gray bars from dark to light colors as time proceeds. Note that such a subperiod does not exclude times of multiple HXR sources or the time with only one bright kernel appeared in a CLEAN map. The vertical dashed line denotes the division between the SXR rise phase and the main/gradual phase in each event. The bottom panel of Figures 1(a)–(d) shows a series of relative positions of two HXR footpoints (plus signs)

with the colors corresponding to the time intervals defined in the upper panel. The origin is set to be the initial location of eastern footpoint and the projection effect has been removed in this plot. The tendency of HXR footpoint motions are indicated by the arrows and numbers. The corresponding neutral line and ribbon morphology are also shown as the dotted and solid curves respectively for comparison. Figures 1(a) and (b) display the clear motion pattern that a parallel/antiparallel movement is followed by a perpendicular movement in conjugate HXR footpoints. Similarly, Figures 1(c) and (d) also display clear motions along the flare ribbons. However, only the western (eastern) footpoint in Figures 1(c) and (1d) shows the systematically perpendicular motion in the subsequent period.

To relate the HXR footpoint motions to the magnetic reconnection process, we calculated the shear angle, which is simply defined as the angle between the line of two HXR footpoints and the line perpendicular to the neutral line, of all the events (21 out of 27) where two distinct HXR footpoints are observed simultaneously and the corresponding neutral line has simple configuration. Based on the assumption that the bright HXR kernels are the conjugate footpoints of newly reconnected magnetic loops, the temporal variations of such shear angle would provide information about the evolution of shear degree of magnetic loops that just reconnected. The larger value of shear angle represents the higher shear degree of magnetic loops. Figures 2(a)–(d) display the time profiles of shear angles in the four events the same as those in Figure 1. The end of the SXR rise phase is indicated
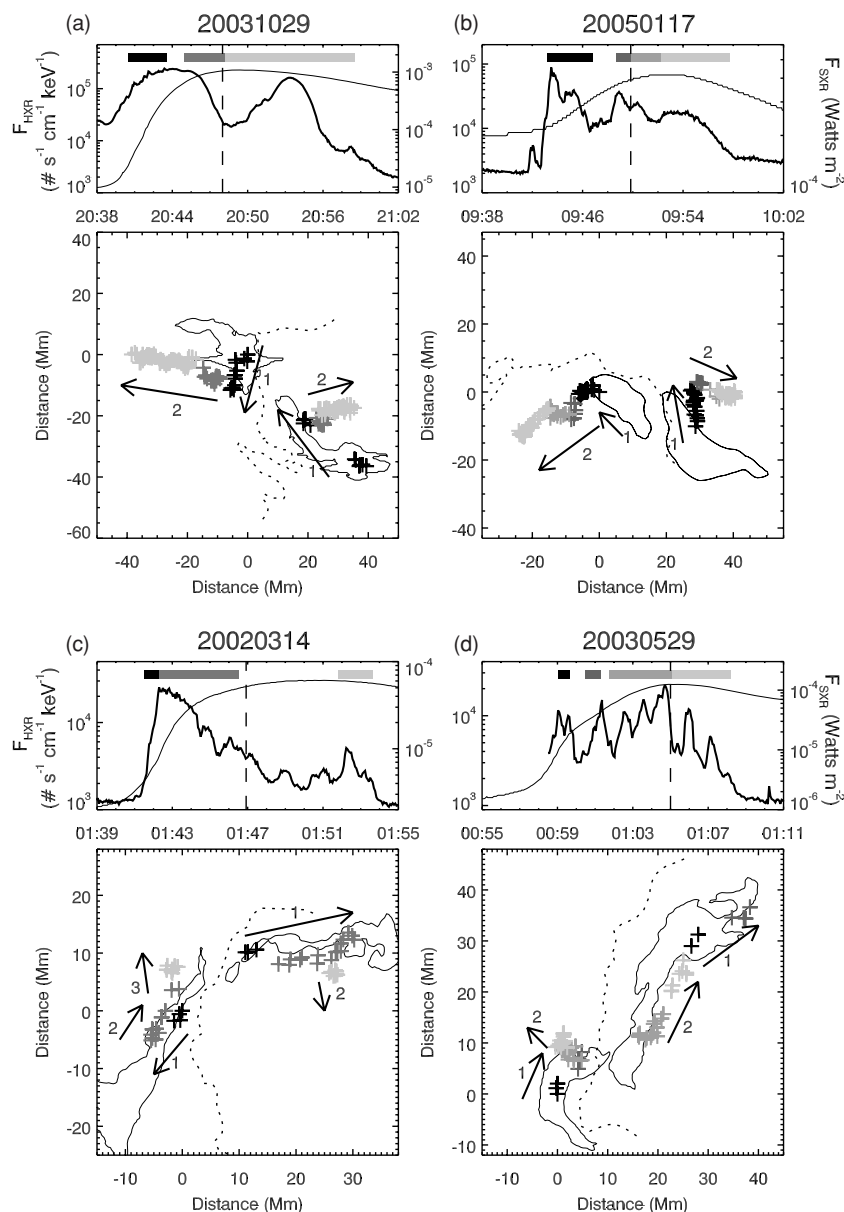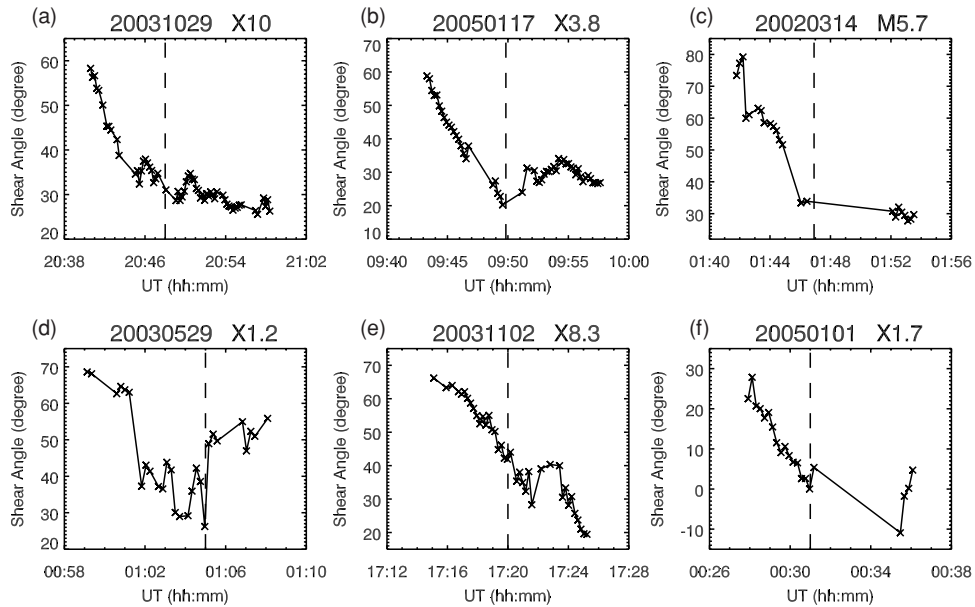
Figure 1. Illustration of HXR footpoint motions from the parallel/antiparallel to the perpendicular motions of the (*a*) X10 flare on 2003 October 29, (*b*) X3.8 flare on 2005 January 17, (*c*) M5.7 flare on 2002 March 14, and (*d*) X1.2 flare on 2003 May 29. (Upper panel) Lightcurves of RHESSI HXR (thick curve) and GOES SXR (thin curve) emissions. The horizontal gray bars from dark to light colors denote the divided time intervals as time proceeds. The end of SXR rise phase is indicated by the vertical dashed line. (Bottom panel) Evolution of HXR footpoints (plus signs) with the corresponding colors in the upper panel. The tendency of HXR footpoint motions are indicated by arrows and numbers. The neutral line and ribbon morphology are shown as the dotted and solid curves, respectively.

by the dashed line. One common feature is found that the shear angle changes significantly in the SXR rise phase, during which the shear angle is large in the beginning and then decreases to a low value at the end of SXR rise phase. In the later flaring period, the value of shear angle and its change are relatively small. Two more events with obvious variations of shear angles are shown in Figures 2(e) and 2(f). Such a time profile of shear angle variation together with the spatial evolution of HXR footpoints indicate that the magnetic reconnection takes place from the inner and highly-sheared magnetic arcade field lines to the outer and weakly sheared arcade field lines. This feature is also found in TRACE observations, as reported in Su et al. (2007).

Other three kinds of complex motion patterns of HXR footpoints are illustrated in Figures 3(a)–(c). The upper panel shows the lightcurves of RHESSI HXR (thick curve) and GOES

SXR (thin curve) emissions, where the divided time intervals are denoted by the horizontal gray bars. The middle panel displays the spatial evolution of conjugate HXR footpoints overlaid by the neutral line (dotted curve) and the contour of ribbons or post-flare loops (solid curve). The tendency of HXR movements is denoted by the arrows (or numbers). The time profile of shear angle is shown in the bottom panel. The vertical dashed lines in the upper and bottom panels indicate the end of the SXR rise phase. In Figure 3(a), both the HXR footpoints move mainly along the neutral line in the same direction throughout the flare but without a significant decrease in shear angle as found in Figure 2. Such a pattern in our study is regarded as large-scale magnetic reconnection taking place along a series of magnetic arcade fields with a localized enhancement of reconnection rate or energy release.

Figure 2. Time profiles of shear angles of the (*a*) X10 flare on 2003 October 29, (*b*) X3.8 flare on 2005 January 17, (*c*) M5.7 flare on 2002 March 14, (*d*) X1.2 flare on 2003 May 29, (*e*) X8.3 flare on 2003 November 2, and (*f*) X1.7 flare on 2005 January 1. The vertical dashed line denotes the end of SXR rise phase.
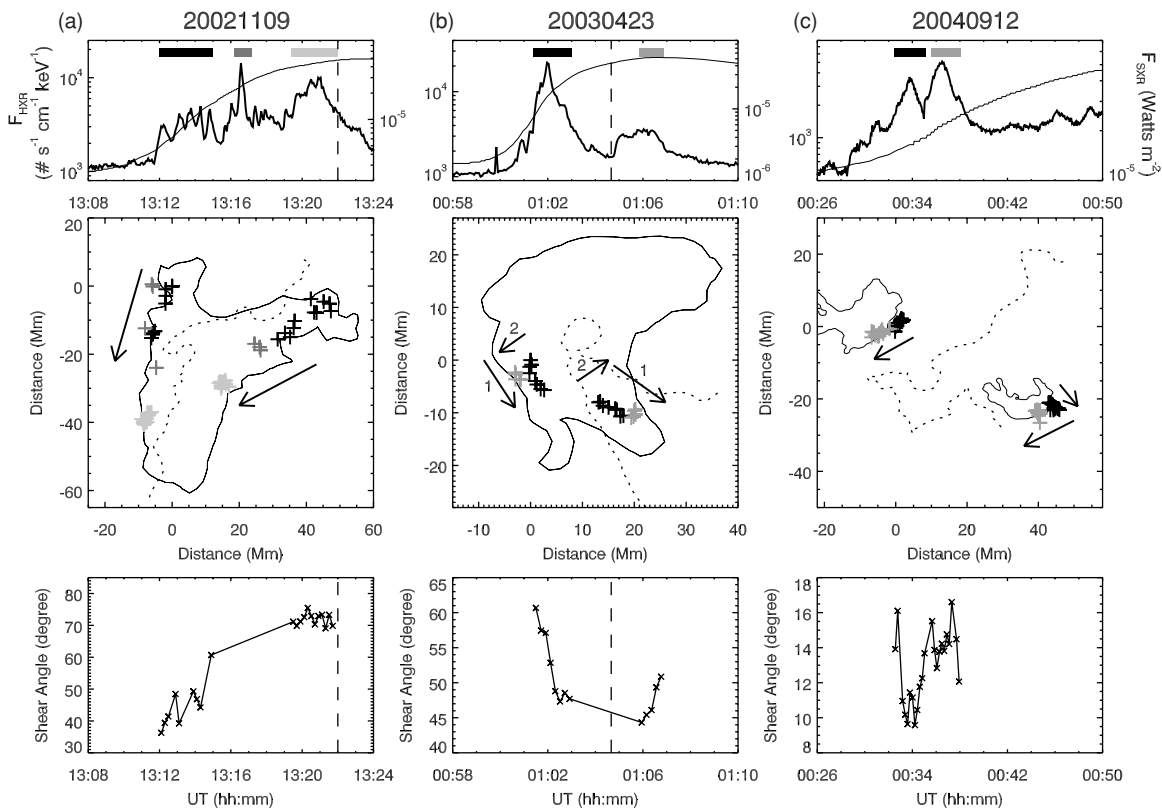
Figure 3. Illustration of other three kinds of complex HXR footpoint motions of the (*a*) M4.6 flare on 2002 November 9, (*b*) M5.1 flare on 2003 April 23, and (*c*) M4.8 flare on 2004 September 12. The solid curves in the middle panel indicate the contours of post-flare loops seen in EIT 195 Å (*a* and *b*) and the ribbon morphology seen in TRACE 171 Å (*c*). (Bottom panel) Time profile of shear angle.

In Figure 3(b), the systematic parallel motion of HXR footpoints with a small amount of shear angle decrease is observed in the SXR rise phase. The HXR footpoints then appear at the farther locations away from the neutral line in the later flaring period. In particular, such a diverging motion corresponds well with the distinct enhancement of HXR emissions, which indicates the magnetic reconnection occurring progressively from the inner

to the outer magnetic arcade field lines as the flare proceeds. On the other hand, the perpendicular motion of HXR footpoints is also observed in the period of each individual HXR emission enhancement. For example, the western HXR footpoint in Figure 3(c) moves away from the neutral line in a nearly perpendicular direction during each enhanced HXR emission, although it displays the parallel motion pattern throughout the
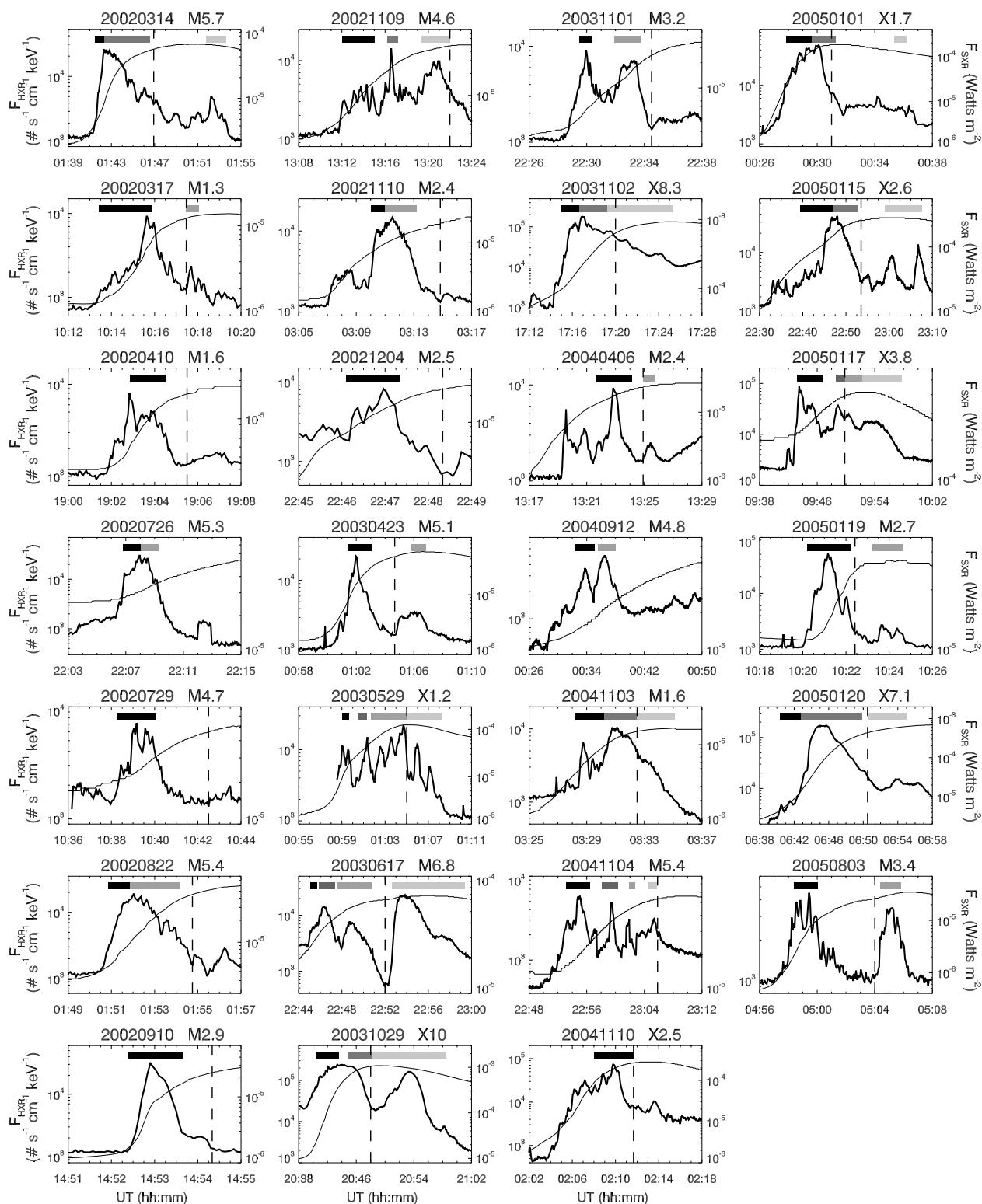
Figure 4. Lightcurves of RHESSI HXR (thick curve) and GOES SXR (thin curve) emissions in all of our 27 events. The horizontal gray bars from dark to light colors in each plot denote the divided time intervals as time proceeds. The end of SXR rise phase is indicated by the vertical dashed line.

flare, while the eastern HXR footpoint moves mainly along the neutral line. The shear angle is almost unchanged during the flare. We suppose that the magnetic reconnection in this flare would take place progressively during each enhancement of HXR emissions resulting in the systematically perpendicular motion of HXR footpoints in smaller spatial scales. Then the subsequent reconnection process in the neighboring magnetic

arcade field lines would be triggered producing the apparent parallel motion of HXR footpoints as time proceeds.

Table 1 lists the observational parameters and the motion patterns of HXR footpoints for all of our 27 events. The first two columns indicate the identification number and the date of each event. The start, peak, and end times measured by GOES $1 \sim 8$ Å are denoted from the third to fifth columns, respectively.

Table 2
Statistical Results of Motion Patterns Throughout Flares

	Parallel/Antiparallel Motion	Perpendicular Motion	Hard to Be Defined
SXR rise phase	74% (20/27)	8% (2/27)	18% (5/27)
SXR main/gradual phase	27% (4/15)	40% (6/15)	33% (5/15)

Table 3
Statistical Results of Motion Patterns for Divided Periods

	Parallel/Antiparallel Motion	Perpendicular Motion
SXR rise phase	74% (59/80)	26% (21/80)
SXR main/gradual phase	43% (12/28)	57% (16/28)

The periods given in the sixth column represent the times when the HXR kernels used for analysis are first and last seen in the reconstructed RHESSI CLEAN maps. The energy band used for reconstructing HXR images are indicated in the seventh column. The associated active region defined by the SEC Solar Event Report and the flare magnitude defined by GOES SXR emissions are recorded in the eighth and ninth columns. The motion patterns in the SXR rise (M_R) and main/gradual (M_{MG}) phases are shown in the tenth column. The following number in the bracket indicates the numbers of divided time intervals in the corresponding phase. In addition, it is worthwhile to relate the motion patterns of HXR footpoints to different flaring phases, which could represent different energy release or acceleration processes during flares. Note that in order to minimize the calculation uncertainty, only the time intervals with systematic HXR footpoint motions are analyzed and counted. The motion patterns for each HXR footpoint in the individual time intervals are recorded in the eleventh (M_{Fp1}) and twelfth (M_{Fp2}) columns. The cross signs indicate motion patterns which are difficult to classify, and could be a random motion, stationary behavior or a perpendicular motion in one footpoint but a parallel motion in the other. The numbers of divided time intervals showing parallel/antiparallel and perpendicular motions in the SXR rise and main/gradual phases are indicated by the four numbers respectively in the last column. Figure 4 displays the lightcurves of RHESSI HXR (thick curves) and GOES SXR (thin curves) emissions in all of our 27 events. The horizontal gray bars from dark to light colors in each plot denote the divided time intervals as time proceeds.

Table 2 summarizes our statistical results by considering the motion patterns of conjugate HXR footpoints simultaneously throughout the flares. We find that in the SXR rise phase, $\sim$ 74% (20 out of 27) flares display the parallel/antiparallel motions and only $\sim$ 8% (2 out of 27) flares show perpendicular motions. The motion patterns of the remaining five events are not easy to identify by a simple classification. However, in the SXR main/gradual phase, the perpendicular motion is more frequently observed ($\sim$ 40%) than the parallel/antiparallel motion ($\sim$ 27%). On the other hand, we also calculate the tendency of HXR footpoint motions by tracing the movement of each footpoint separately in each divided time interval, as summarized in Table 3. It is obvious that the pattern of parallel/antiparallel motion dominates ($\sim$ 74%) in the SXR rise phase; while the perpendicular motion becomes dominated ($\sim$ 57%) in the SXR main/gradual phase. This is the first result quantitatively recognizing the preference of temporal evolution of HXR footpoints by investigating their motion patterns throughout the HXR flaring periods as well as in the individual time intervals of enhanced HXR emissions.

4. DISCUSSION AND SUMMARY

The purpose of this study is to recognize the tendency and the preference of flare-related HXR footpoint motions by analyzing the temporal and spatial evolution of RHESSI HXR kernels combined with the corresponding neutral line obtained from MDI magnetograms and the ribbon morphology seen in EUV/UV or Hα. A total of 27 M- and X-class flares are analyzed based on the motions predominantly parallel/antiparallel and predominantly perpendicular to the neutral line or ribbons. Four kinds of systematic motion patterns are presented and their relationships to the possible magnetic reconnection processes are described as well by regarding the HXR kernels as the chromospheric footpoints of newly reconnected field lines in corona. Besides, we also estimate the shear angles of 21 events, where two distinct HXR footpoints are observed simultaneously and the configuration of neutral line is simple enough to be represented by a straight line.

A clear two-step motion pattern of HXR footpoints, namely, moving mainly along a neutral line or ribbons in the SXR rise phase of flares and then separating from each other in the nearly perpendicular direction in the SXR main/gradual phase, is observed and illustrated in Figure 1. A common feature that the shear angle decreases significantly in the SXR rise phase is also found in such flares. It is thus interpreted as the progression of magnetic reconnection from the inner and highly-sheared arcade fields to the outer and weakly sheared field lines as the flare proceeds. The preference of HXR kernels appearing at the footpoints of highly-sheared magnetic loops at the start of the SXR rise phase is consistent with the magnetic reconnection theory that the reconnection occurring at sheared magnetic arcade field lines produces most HXR energy release in the impulsive phase of large flares. Furthermore, the observation of such two-step motion pattern of HXR footpoints is consistent with the simulation result by Choe & Cheng (2000) that the magnetic reconnection process would cease when the shearing footpoint motion is followed by a diverging motion. Other three kinds of complex motion patterns of HXR footpoints are illustrated in Figure 2. A systematic parallel motion of HXR footpoints along the neutral line is not only observed throughout the HXR flaring period (Figure 2(a)), but also observed during each individual enhancement of HXR emissions together with perpendicular motion in various ways (Figures 2(b) and (c)). We suppose

that the magnetic reconnection in the flares which have large displacements of HXR footpoints throughout the HXR flaring period could take place along a series of magnetic loops but enhances in some localized regions coinciding with the positions of HXR kernels. In addition, we also find the recurrence of the same motion pattern of HXR footpoints in some flares, such as the movements shown in Figure 2(c), which represents the recurrence of the same magnetic reconnection process during a flare. Moreover, by considering the motion patterns of conjugate HXR footpoints simultaneously throughout the flares, we find that $\sim 74\%$ of our 27 flares in the SXR rise phase show parallel/antiparallel motions. However, perpendicular motion is more frequently observed ($\sim 40\%$) in the SXR main/gradual phase than the motions along neutral line or ribbons ($\sim 27\%$). This is the first time that the temporal evolution of flare-related HXR footpoint motions is quantitatively demonstrated.

On the other hand, it is interesting to mention that unlike the well-identified two-ribbon structures in EUV/UV or Hα observations, the HXR sources in large flares usually appear as kernels with asymmetric HXR emissions in two conjugate footpoints of reconnected magnetic field lines and sometimes even multiple kernels are observed simultaneously. The ribbon-like HXR structure is rarely observed, with the exception of only one Yohkoh event (Masuda et al. 2001) and one RHESSI event (Liu et al. 2007), and is usually attributed to the limitation of dynamic ranges in HXR instruments. Unlike the well separated two HXR footpoints, we suppose that the ribbon-like HXR structure would result from the multiple magnetic reconnection processes that take place simultaneously along a series of magnetic loops. The positions of HXR kernels inside the ribbon-like structure represent the sites of localized enhancement in magnetic reconnection or energy release. Jing et al. (2007) compare the spatial distribution of HXR intensity with the local magnetic reconnection rate and energy release rate of the M8.0 flare on 2005 May 13, which is the same event as discussed in Liu et al. (2007), by estimating the expansion speed of Hα ribbons and the strength of magnetic fields swept by the ribbons. They found that the HXR intensity distribution shows a good spatial correlation with the reconnection rate and energy release rate when the HXR sources appear as kernels. However, such correlation is decreased when the HXR sources evolve to the ribbon-like structure. More detailed investigation about the spatial distribution of reconnection rate or energy release rate along the ribbon-like HXR structure and the temporal evolution of reconnection electric field from kernel to ribbon-like structures will be addressed in the future.

We must point out that it is difficult to explain all the observational HXR motion patterns by using only one flaring model. Comparisons with modeling or simulation would be useful to clarify the magnetic reconnection process. Moreover, the following questions are still not understood: (1) what dominate(s) the preference of motion pattern along or perpendicular to the neutral line and (2) what result(s) in the transition in these two motions. More detailed investigation about the relationship between motion patterns and physical parameters (e.g., magnetic magnitude, arcade size, or relative velocity between two conjugate HXR footpoints) derived from modeling or simulation would be worthwhile to do in the future.

REFERENCES

Bogachev, S. A., & Somov, B. V. 2005, ApJ, 630, 561
Carmichael, H. 1964, in The Physics of Solar Flares, ed. W. N. Hess (NASA SP-50; Washington, DC: NASA), 451
Choe, G. S., & Cheng, C. Z. 2000, ApJ, 541, 449
Fletcher, L., & Hudson, H. S. 2002, Sol. Phys., 210, 307
Grigis, P. C., & Benz, A. O. 2005, ApJ, 625, L143
Hirayama, T. 1974, Sol. Phys., 34, 323
Hurford, G. J., et al. 2002, Sol. Phys., 210, 61
Ji, H., Huang, G., Wang, H., Zhou, T., Li, Y., Zhang, Y., & Song, M. 2006, ApJ, 636, L173
Jing, J., Lee, J., Liu, C., Gary, D. E., & Wang, H. 2007, ApJ, 664, L127
Kopp, R. A., & Pneuman, G. W. 1976, Sol. Phys., 50, 85
Kosugi, T., et al. 1991, Sol. Phys., 136, 17
Krucker, S., Fivian, M. D., & Lin, R. P. 2005, Adv. Space Res., 35, 1707
Krucker, S., Hurford, G. J., & Lin, R. P. 2003, ApJ, 595, L103
Lin, R. P., et al. 2002, Sol. Phys., 210, 3
Liu, C., Lee, J., Gary, D., & Wang, H. 2007, ApJ, 658, L127
Liu, W., Jiang, Y. W., Liu, S., & Petrosian, V. 2004, ApJ, 611, L53
Masuda, S., Kosugi, T., & Hudson, H. S. 2001, Sol. Phys., 204, 55
Priest, E. R., & Forbes, T. G. 2002, A&A Rev., 10, 313
Sakao, T., Kosugi, T., & Masuda, S. 1998, in Observational Plasma Astrophysics: Five years of Yohkoh and Beyond, ed. T. Watanabe, T. Kosugi, & A. C. Sterling (Dordrecht: Kluwer), 273
Siarkowski, M., & Falewicz, R. 2004, A&A, 428, 219
Smith, D. M., et al. 2002, Sol. Phys., 210, 33
Sturrock, P. A. 1966, Nature, 211, 695
Su, Y., Golub, L., & Van Ballegooijen, A. A. 2007, ApJ, 655, 604
Veronig, A. M., Karlický, M., Vrnak, B., Temmer, M., Magdalenić, J., Dennis, B. R., Otruba, W., & Pötzi, W. 2006, A&A, 446, 675